

Unusual Behavior of the Bipolar Molecule 25-Hydroxycholesterol at the Air/Water Interface—Langmuir Monolayer Approach Complemented with Theoretical Calculations

Anita Wnętrzak, Anna Chachaj-Brekiesz, Jan Kobierski, Katarzyna Karwowska, Aneta D. Petelska, and Patrycja Dynarowicz-Latka*

Cite This: *J. Phys. Chem. B* 2020, 124, 1104–1114

Read Online

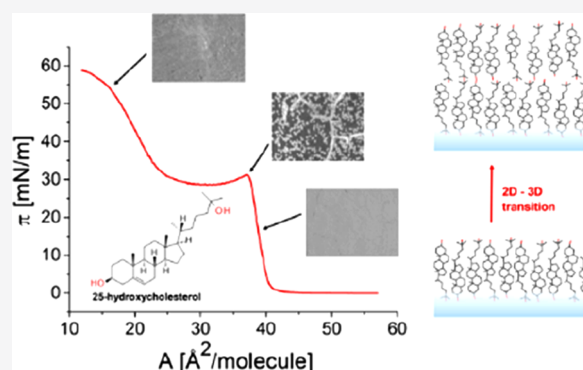
ACCESS |

Metrics & More

Article Recommendations

Supporting Information

ABSTRACT: In this study, 25-hydroxycholesterol (25-OH), a biamphiphilic compound with a wide range of biological activities, has been investigated at the air/water interface. We were interested in how two hydroxyl groups attached at distal positions of the 25-OH molecule (namely, at C(3) in the sterane system and at C(25) in the side chain) influence its surface behavior. Apart from traditional Langmuir monolayers, other complementary surface-sensitive techniques, such as electric surface potential measurements, Brewster angle microscopy (BAM), enabling texture visualization and film thickness measurements), and polarization modulation-infrared reflection-absorption spectroscopy (PM-IRRAS), were applied. Experimental data have been interpreted with the aid of theoretical study. Our results show that 25-OH molecules in the monomolecular layer are anchored to the water surface alternatively with C(3) or C(25) hydroxyl groups. Theoretical calculations revealed that the populations of these alternative orientations were not equal and molecules anchored with C(3) hydroxyl groups were found to be in excess. As a consequence of such an arrangement, surface films of 25-OH are of lower stability as compared to cholesterol (considered as a non-oxidized analogue of 25-OH). Moreover, it was found that, upon compression, the transition from mono- to bilayer occurred. The molecular mechanism and interactions stabilizing bilayer structure were proposed. The explanation of the observed unusual surface behavior of 25-OH may contribute to an understanding of differences in biological activity between chain- and ring-oxidized sterols.



1. INTRODUCTION

Bipolar molecules have been of constant interest from the early stage of floating monolayers investigations in the times of Langmuir to the present day. Initial research was focused on their different behavior on the water surface depending on the position of the polar groups in the molecule. Aliphatic molecules having either identical (alkyl diols,¹ dicarboxylic acids,^{2,3} diammonium halides,⁴ aromatic amines⁵) or different polar groups (like hydroxycarboxylic acids^{6–13}) have been studied most frequently. For both kinds of bipolar molecules, the same monolayer behavior was observed. Namely, when polar groups were placed in an adjacent position, they were acting as a common entity and the characteristics of their Langmuir monolayers resembled those for monopolar amphiphiles.^{1–3} The high monolayer stability has suggested that they are anchored with both polar groups in the water surface and their orientation does not change with the compression.² However, when polar groups were located further away so that a headgroup is present on each end of a hydrophobic skeleton, like for α,ω -bipolar compounds (ref 2 and references therein^{6,7,9–15}) (referred to as “bolaamphim-

philes”, “bolas”, “bolytes”, or “bolaform amphiphiles”), such molecules were found to behave differently. As discussed in ref 16, at large areas per molecule, they adopt a flat (horizontal) to the water surface orientation. Upon compression, depending on the character of a polar group (charged or not; its polarity and size) and the structure of the hydrophobic part (single chain or macrolide structure), they can either bend, forming loops (“wicket” conformation; also referred to as a “horseshoe” arrangement⁶), or they can lift one group from the water surface, and the molecule assumed a vertical orientation, which was responsible for the observed instability of their monolayers.² In some cases, both conformations may coexist, as reported in ref 17.

Recently, the increase of interest in bipolar amphiphiles has been associated with molecules of biomedical importance.

Received: November 22, 2019

Revised: January 14, 2020

Published: January 23, 2020

Special interest has been devoted to cholesterol oxidation products, so-called oxysterols, which play important roles in the organisms (for a review, see ref 18). Oxysterols contain—as compared to cholesterol—additional (one or more) oxygen-containing functional groups, for example, hydroxyl, carbonyl, carboxyl, or epoxy moieties.¹⁹ Depending on their route of formation, i.e., non-enzymatic or enzymatic, the additional polar group is placed either in the ring or in the side chain, respectively.²⁰

Although—at first sight—the structure of cholesterol and oxysterols seems to be similar, their arrangement in biological membranes can differ significantly. The orientation of cholesterol has well been described using the Langmuir monolayer as a membrane-mimicking model;²¹ i.e., in a phospholipid environment, cholesterol molecules are oriented vertically to the membrane plane with its hydrophobic part aligned parallel to phospholipid acyl chains. However, the presence of an additional polar group, either in the ring or in the side chain, may change the alignment of molecules and thus modify both polar and hydrophobic interactions with membrane phospholipids and change membrane physicochemical properties and its functioning.

The arrangement of chain-oxidized cholesterol is interesting. A horizontal orientation of molecules anchored with both OH groups to the water surface²¹ was formerly suggested based on bolaamphiphiles having a polymethylene chain linking two polar groups located in a distal position. Such molecules, exemplified by hydroxystearic acids,¹² were found to adopt a “looping” conformation, where both polar groups were in contact with the water subphase in an expanded monolayer. Upon compression, one polar group (in this particular case, a hydroxyl group, which is weaker hydrophilic) detaches from the surface, and this orientation change is signaled by the presence of a plateau in the course of the π/A isotherm. However, for chain-oxidized sterols, such an arrangement is doubtful, considering a very stiff sterane moiety that prevents the formation of a “horseshoe” conformation. In this paper, we have undertaken the challenge to understand the arrangement of a selected chain-oxidized cholesterol, namely, 25-hydroxycholesterol (in short, 25-OH), in artificial membrane modeled with the Langmuir monolayer technique. We hope that the results of our investigation help to understand the different biological activities of ring-oxidized versus chain-oxidized sterols.

2. MATERIALS AND METHODS

2.1. Materials. 25-Hydroxycholesterol (25-OH) and cholesterol (Chol) were provided by Avanti Polar Lipids in purity >99% and used without extra purification. Chloroform and methanol, characterized by high purity ($\geq 99\%$, Chempur, Poland), were used to clean the Langmuir trough. Spectroscopic grade chloroform (purity $\geq 99.9\%$, POCh, Poland), containing ethanol as a stabilizer, was used to prepare spreading solutions of 25-OH. Water, used as a subphase, was purified by a Millipore system, giving a product with a resistivity of 18.2 M Ω -cm and a surface tension of 72.8 mN/m at 20 °C.

2.2. Methods. **2.2.1. Langmuir Monolayer Technique.** The investigated oxysterol was dissolved in chloroform at a concentration of 10^{-3} mol/dm³. Langmuir monolayers were obtained by spreading the aliquot of the above-mentioned solution with a Hamilton microsyringe (precise to ± 2.5 μ L) onto the surface of ultrapure water. A Langmuir film balance

with uniaxial compression, NIMA 301S (single barrier, total area = 300 cm²) or NIMA 612D (double barrier, total area = 600 cm²), was used to record the pressure (π)/area (A) isotherms. Surface pressure was measured with an accuracy of 0.1 mN/m using a Wilhelmy plate made from ashless chromatography paper (Whatman Chr1) as the surface pressure sensor. Each isotherm was repeated at least three times to ensure reproducibility of the curves to ± 2 \AA^2 /molecule. To provide a detailed Langmuir monolayer characterization, experiments under different conditions (i.e., subphase temperature, barrier speed, number of molecules deposited on the surface) were performed. The monolayer kinetics was verified with compression–expansion cycles to different surface pressure values (20 and 40 mN/m). The stability of the film was checked at different surface pressure values: 10, 20, and 40 mN/m for 60 min. Surface potential measurements were performed with the Kelvin probe (model KP2, NFT) mounted on a NIMA 612D trough. The vibrating plate was located ca. 1–2 mm above the water surface, while the reference electrode (platinum foil) was placed in the subphase. The surface potential measurements were reproducible to ± 15 mV.

2.2.2. Brewster Angle Microscope. Visualization of the texture of the floating 25-OH monolayer as well as film thickness measurements were carried out using an ultraBAM instrument (Accurion GmbH) installed over a KSV 2000 (double barrier, total area = 700 cm²) Langmuir device. Minimum reflection was set with a p-polarized laser beam ($\lambda = 658$ nm) incident on the pure aqueous surface at the Brewster angle (53.15°). The Langmuir monolayer was prepared as described above. Light reflected from the monolayer was collected through a 10 \times objective and lens system to a CCD camera. Brewster angle microscopy (BAM) images presented in this paper show monolayer fragments of 720 μ m \times 400 μ m. The gray level at each pixel characterizes reflectivity which, in turn, can be transformed into the optical thickness of the monolayer.^{22,23}

2.2.3. PM-IRRAS and ATR-FTIR Spectroscopy. PM-IRRAS spectra of monolayers on an aqueous subphase compressed to the selected surface pressure values were obtained using the KSV PM-IRRAS instrument at an angle of incidence of 80°. Each spectrum was a result of 6000 scans accumulated with a spectral resolution of 8 cm⁻¹. Measurements were performed at least two times to ensure reproducibility of the results. The obtained spectra were processed with OPUS software: background subtraction, baseline correction (straight lines, 1 \times), and smoothing (Savitzky–Golay method).

The ATR-FTIR (attenuated total reflection Fourier transform infrared) spectrum of 25-OH in the range 4000–600 cm⁻¹ was measured with a Nicolet Almega microscope system fitted with a single bounce diamond micro-ATR with the diamond top plate option. For each spectrum, 64 scans were co-added with a spectral resolution of 4 cm⁻¹.

2.2.4. Theoretical Calculations. **2.2.4.1. IR Spectra Calculations.** Geometry optimization and frequency calculations of 25-OH molecule were performed using density functional theory (DFT) modeling through the Gaussian 16 software package.²⁴ All calculations were performed using the B3LYP functional^{25–28} with a 6-311+G(d,p) basis set. Systems were optimized using the default UltraFine integration grid, default integer values, and a combination of EDIIS and CDIIS tight convergence procedures, with no damping or Fermi broadening. The raw frequencies obtained from the vibrational

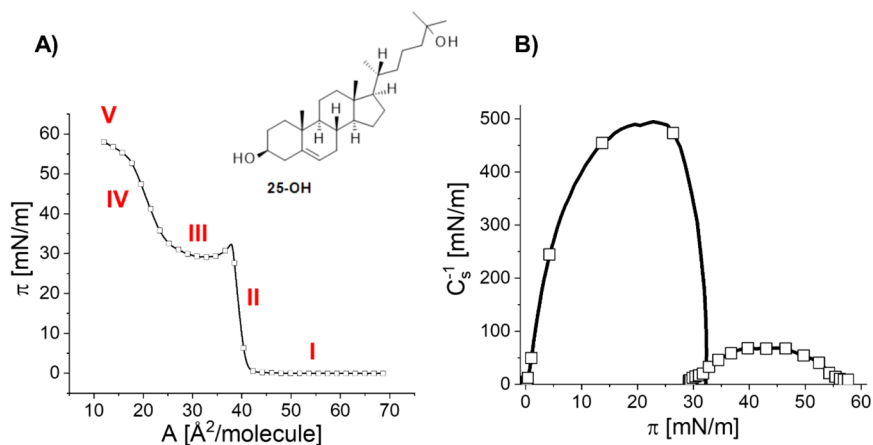


Figure 1. Surface pressure–area isotherms (A) and compressibility modulus (B) for 25-OH recorded at 20 °C. Inset: structural formula of 25-OH.

simulation were scaled by a factor of 0.967.²⁹ The base superposition error (BSSE) for the calculations of dimer energy was eliminated by using the Counterpoise option.

2.2.4.2. Molecular Dynamics. The electrostatic potential for previously optimized 25-OH was calculated in Gaussian 16 using the B3LYP/6-31G(d) method. RESP fitting was conducted in Antechamber³⁰ using the general Amber force field (GAFF).³¹ Completeness of the parameters was checked in the Parmchk2 program. The molecules were packed in boxes using Packmol.³² The TIP3P model was used to simulate water molecules.³³ Molecular dynamics was calculated in the Amber 2018 software.³⁴ Periodic box conditions were used. The energy of the systems was minimized by 50,000 steps. Systems were equilibrated by 75,000 steps with a 0.001 ps time step, followed by 300,000 steps with a 0.002 ps time step. Production calculations were carried out under the isothermal–isobaric ensemble with constant surface tension ($NP\gamma T$) with a 0.002 ps time step. Long-range electrostatic interactions were taken into account using a particle mesh Ewald method with 12 \AA and a force switching region above 10 \AA . A Langevin thermostat was used with the temperature set at 293.15 K. A Berendsen barostat was used to control the pressure at 1 bar. Each of the systems used in the molecular dynamics of monolayers consisted of two monolayers, each having 128 differently oriented 25-OH molecules, separated by 30,000 water molecules. To avoid the interaction between monolayers, 100 \AA of vacuum was left in the Z direction between adjacent periodic boxes. The molecular dynamics of self-assembling systems of cholesterol in water and 25-OH in water were performed from a random mixture of these molecules. Each system consisted of 256 molecules of cholesterol or 25-OH and 7680 molecules of water (which corresponds to 30 molecules of water per molecule of lipid). A lipid14 force field was used for cholesterol.³⁵ Results of molecular dynamics were visualized in VMD.³⁶ Electron density functions and radial pair distribution functions were determined in the Cpptraj program.³⁷

3. RESULTS AND DISCUSSION

3.1. Surface Pressure–Area Isotherms. In the first step of our studies, the surface characteristics of the biamphiphilic sterol 25-OH were examined, and the representative π – A isotherm is shown in Figure 1. In Supporting Information (Figure S1), for comparison, the same isotherm is combined with the isotherm of cholesterol (bearing one hydroxyl group

at C(3) in the sterane system) and 25-OH³⁸ (bearing one hydroxyl group at C(25) in the side chain).

The registered π – A curve for 25-OH starts to rise rapidly at the area per molecule value of about 43 $\text{\AA}^2/\text{molecule}$, and the inclination of the isotherm is similar to that observed for cholesterol (Supporting Information, Figure S1). The value of the onset area of surface pressure (*lift-off* area) suggests that the 25-OH molecule, similarly to cholesterol and 25-OH', is anchored to the water surface with only one hydroxyl group; otherwise, the *lift-off* area would be noticeably larger. At a surface pressure of about 32.5 mN/m, a characteristic *kink* appears, followed by a pseudo-plateau region. Upon further compression, the pressure starts to rise again, attaining a surface pressure of almost 60 mN/m. 25-Hydroxycholesterol was already investigated in Langmuir monolayers, but its isotherm can be found in only a few papers.^{39–41} However, none of these works show a full compression isotherm.

To better understand the in-plane surface elasticity of a monolayer, the compressibility modulus (C_s^{-1}) was calculated from the isotherm's data points, using the formula $C_s^{-1} = -A \left(\frac{d\pi}{dA} \right)$.⁴² Looking at Figure 1B, it can be noticed that the compressibility modulus vs π dependence for 25-OH is characterized by two maxima: the first one of $C_s^{-1} \approx 500 \text{ mN/m}$ (corresponding to the solid state) and the second one of $C_s^{-1} \approx 70 \text{ mN/m}$. A notable drop of C_s^{-1} to zero may indicate that between these two phases a transition, associated with the formation of the 3D phase, occurs.⁴³ Taking into consideration the lower value of C_s^{-1} observed for the phase existing above the pseudo-plateau region, we first supposed that the second rise observed in the isotherm is associated with the formation of random 3D aggregates. However, after careful study, we found this pseudo-plateau region of the isotherm (III) highly reproducible (Supporting Information, Figure S2). This encouraged us to conduct further experiments to get insight into the origin of this transition. First, the effect of various experimental conditions was examined. We found that the type of compression (symmetrical or unilateral) (Supporting Information, Figure S3), the barrier material (Delrin or Teflon) (Supporting Information, Figure S3), and the number of spread molecules (Supporting Information, Figure S2) practically do not affect the course of the isotherm. Interestingly, the orientation of the Wilhelmy plate (parallel or perpendicular) with respect to barrier position (Supporting Information, Figure S4) has a

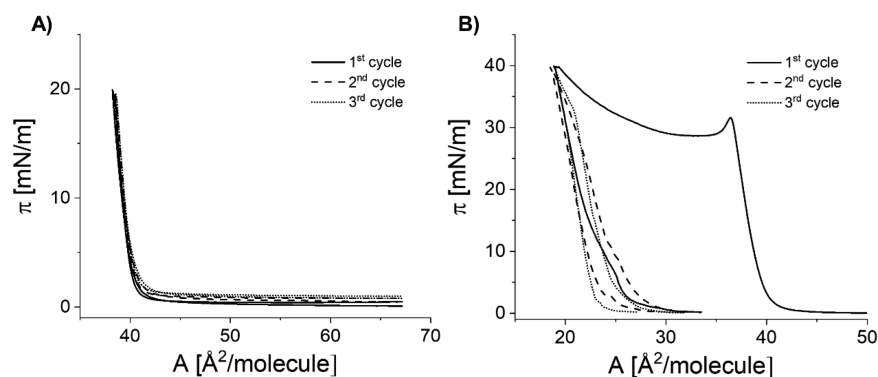


Figure 2. Isotherms of compression–expansion cycles registered for 25-OH at 20 °C for compression to different surface pressure values: 20 mN/m (A) and 40 mN/m (B).

significant influence on the shape of regions IV and V of the isotherm. Furthermore, the isotherm from 25-OH seems to not be affected by the speed of compression (Supporting Information, Figure S5), except for a very slow rate (5 cm²/min), causing a slight shift of the plateau and high pressure regions (IV and V) to lower π values. Taking into consideration the above-mentioned findings, we used the following conditions in routine experiments: double Delrin barriers, compression speed of 20 cm²/min, the parallel orientation of the Wilhelmy plate with respect to barrier position, and subphase temperature of 20 °C (otherwise specified). Interestingly, the monolayer formed by 25-OH is of lower stability (Supporting Information, Figure S6) as compared to cholesterol, which has been found to form very stable monolayers at both low and high pressure regions.^{44,45} After reaching the desired surface pressure and stopping the compression, π drops rapidly to about 70% of its initial value and then stabilizes with time. The highest film stability is observed in the low pressure region (10 mN/m).

Compression–expansion cycles showed no hysteresis for films compressed to a surface pressure of 20 mN/m (region II), whereas pronounced hysteresis was observed at a higher surface pressure of 40 mN/m (region IV) (Figure 2). As can be seen in Figure 2b, the experimental curves registered during the second and third cycles are strikingly different (both in shape and in the onset area) as compared to the first compression cycle. This suggests that the formation of the phase observed at high surface pressures above the plateau (isotherm region IV) is irreversible.

In the next step, we examined how temperature influences monolayers from 25-OH (Figure 3).

The increase of temperature lowers the pressure of the plateau region and decreases the pressure of the *kink*. Such a temperature dependence inverted to that of a transition originating from phase coexistence^{46–48} can be attributed to the transition of a monolayer into a 3D collapsed state. To look deeper into the observed transition, microscopic (Brewster angle microscopy, BAM) spectroscopic (polarization modulation-infrared reflection-absorption spectroscopy, PM-IRRAS), and electric (surface potential, ΔV) measurements were applied.

3.2. Brewster Angle Microscopy. BAM experiments allow direct observation of the film's texture. Additionally, the BAM instrument, equipped with the gray level measurement mode, enables the *optical thickness* of the film to be determined (Figure 4A). Figure 4B shows representative images of the observed surface textures.

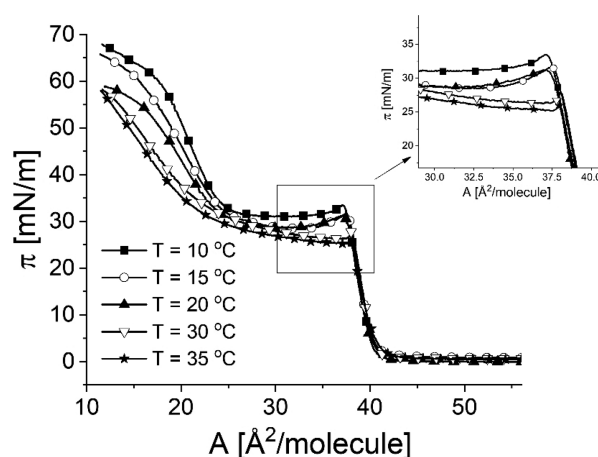


Figure 3. Temperature dependence of surface pressure–area isotherms for 25-OH.

At the initial step of compression, below 1 mN/m, the texture of the film is typical for gas–liquid coexistence (Figure 4B, image a). Then, upon compression, the observed condensed-phase domains are getting closer to each other and partly merge (image b). In consequence, the film becomes more homogeneous; however, dark borders between large fragments are still noticeable (image c). When the isotherm reaches the *kink*, bright objects appear as nuclei and most of them arrange in the form of long and narrow filaments (in the places where dark borders were previously observed)—image d. Upon further compression, the filaments break and the growth of small bright domains occurs—image e. This process continues as the isotherm passes through the plateau region (image f). When the compression proceeds and molecular packing increases, the voids (seen as dark areas) become smaller (image g). Finally, the texture becomes thicker without visible discontinuities (images h), which suggests the formation of multilayer structures.

At the same time, the *optical thickness* of the Langmuir film was recorded (see Figure 4A). Since the refractive index of a film composed of 25-OH is unknown, we assumed its value equal to the refractive index of cholesterol (1.47).²² As can be noticed, the monolayer thickness during the first rise of surface pressure reaches a value of ca. 2.35 nm, which corresponds to a single layer of 25-OH molecules anchored to the surface of the water with one hydroxyl group. While the film is further compressed, the thickness rises to ca. 4 nm and remains fairly constant in the IV and V regions. The 2-fold increase in film

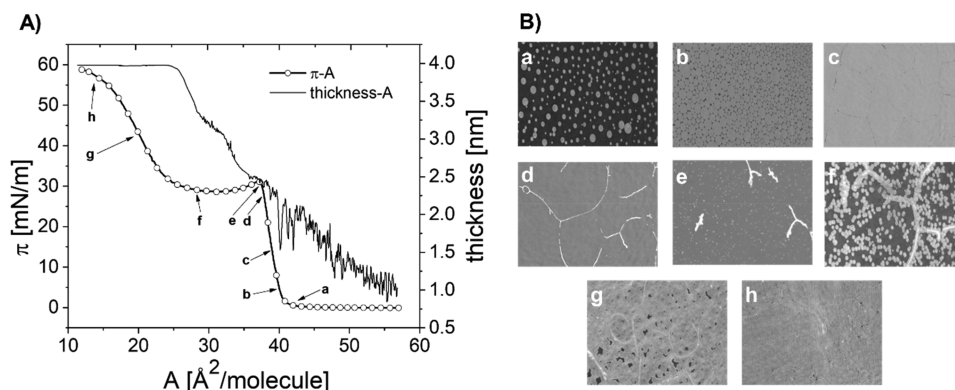


Figure 4. Surface pressure–area isotherm and thickness versus area per molecule plot for the 25-OH monolayer spread on the water at 20 °C (A). Textures of 25-OH films on the water subphase registered with BAM at different values of surface pressure. The isotherm regions corresponding to each texture are marked with corresponding letters (a–h) (B).

thickness (between regions III and IV) suggests that 25-OH forms a bilayer at the surface of the water, and therefore, the observed plateau region is due to a transition from mono- to bilayer structure. This is additionally supported by the isotherm, since the ratio of the area/molecule values at the beginning and end of the plateau region is close to 2. For Langmuir monolayers, such behavior is uncommon. Typically, rigid monolayers upon compression to areas below their geometrical size undergo random collapse involving either folding processes (leading to tri-layered structures)⁴⁹ or 3D aggregate formation.^{50,51}

Additionally, *optical thickness* and BAM images were registered during a compression–expansion cycle analogical to that shown in Figure 2B (Supporting Information, Figure S7). During expansion, the surface layer becomes discontinuous and cracked (Supporting Information, Figure S7B and C), while the thickness of film fragments remains similar to that measured upon compression for the bilayer. The obtained results confirm that the monolayer–bilayer transition is irreversible.

It seems that in the case of 25-OH the transition from mono- to bilayer structure is stabilized due to the unique structure of this compound, namely, the presence of two hydroxyl groups localized at the opposite sites of the molecule. To support this hypothesis, electric surface potential measurements were carried out.

3.3. Surface Potential–Area Isotherms. Semiempirical analysis of the measured electric surface potential, ΔV , has been done using the Helmholtz equation, $\Delta V = \mu_{\perp} / (A \cdot \epsilon \cdot \epsilon_0)$,⁵² where μ_{\perp} is the vertical component of the dipole moment (called the *effective dipole moment*) of a film molecule, ϵ_0 is the vacuum permittivity, and ϵ is the permittivity of the monolayer. Since the value of ϵ is unknown, the changes of effective dipole moment upon compression can be represented by the apparent dipole moment, $\mu_a = \mu_{\perp} / \epsilon$.

As can be seen in Figure 5, at large areas per molecule, the surface potential and apparent dipole moment remain approximately constant until they reach 62 Å (so-called *critical area*^{53,54}). Then, the slope of the curves starts to increase, strikingly evidencing changes in the orientation of molecules. For areas per molecule corresponding to bilayer formation (about 40 Å), the inflection of the curves is observed: the ΔV – A curve rises with a smaller slope, whereas the μ_a – A curve sharply decreases. This suggests depolarization of the surface film, which results from bilayer formation; i.e., dipole moments

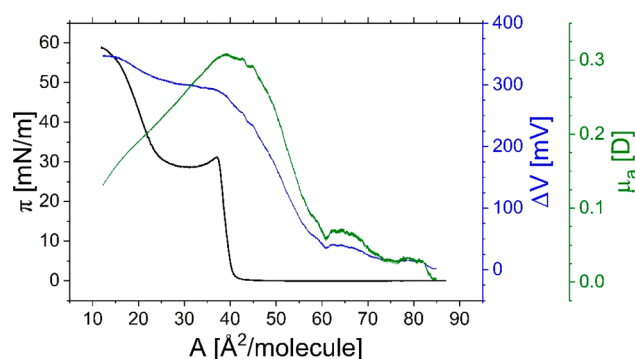


Figure 5. Surface pressure, surface potential, and apparent dipole moment versus area per molecule plots for 25-OH film spread on the water at 20 °C.

of molecules from the upper layer compensate those arising from molecules underneath.

3.4. PM-IRRAS Spectra. PM-IRRAS is a surface-sensitive technique which, due to its special selection rules, enables one to (i) estimate film thickness⁵⁵ as well as describe molecular orientation⁵⁶ and (ii) obtain information on functional groups involved in intermolecular interactions.⁵⁷ This makes PM-IRRAS a suitable, complementary tool for investigating the surface behavior of 25-OH monolayers, including the formation of bilayers at the water surface.

In the initial step of our spectroscopic research, the theoretical IR spectrum of 25-OH was calculated using the B3LYP method and 6-311++G(d,p) basis set. In the spectral region below 3000 cm^{-1} , the obtained results are in agreement with the recorded experimental ATR-FTIR spectrum from the bulk (for comparison, see Supporting Information, Figure S8) and enabled us to assign selected bands to molecular vibrations as well as determine the orientation of the dipole moment vector with respect to the long axis of the 25-OH molecule (Table 1).

In the next step of our spectroscopic studies, we analyzed PM-IRRAS spectra in two selected regions, 3000–2825 cm^{-1} (Figure 6, panel A) and 1500–1325 cm^{-1} (Figure 6, panel B), where bands from stretching and scissoring vibrations in hydrocarbons are observed, respectively. PM-IRRAS spectra were recorded at different surface pressure values.

Generally, it can be noticed that PM-IRRAS spectra show similar courses as compared to experimental and theoretical curves from the bulk; however, PM-IRRAS bands seem to be

Table 1. Frequencies (in cm^{-1}) and Assignments of Important Vibrations of 25-OH

scaled frequency ^a (cm^{-1})	observed frequency (cm^{-1})		description of the vibration
	ATR-IR (bulk sample)	PM-IRRAS (monolayer)	
1017	1021	1016–1020	rings deformation
1035	1040	1035–1045	C(3)—O stretching; C—C—C scissoring in rings
1054	1054	1054 (at 20 mN/m)	C—O—H scissoring (both)
1068			rings deformation; CH_2 twisting in rings
1073		1077–1082	
1116	1009	1009	C(25)—O—H scissoring; CH_2 rocking; C—C—C scissoring at the end of the chain
1140	1141	141 (at 10 mN/m)	CH_2 twisting; rings deformation
1164	1158	1167–1170	CH_2 twisting; C=C—C scissoring; rings deformation
1196	1195	1192	C(25)—O stretching
1231	1233	1232	CH_2 wagging in chain
1277	1277	1272	C(3)—O—H scissoring; CH_2 wagging in rings
1310	1316	1310–1316	C(25)—O—H scissoring
1335	1333		C(25)—O—H scissoring; CH_2 wagging in chain
1351	1362	1350	CH_3 scissoring
1371	1376	1378–1383	
1425			CH_2 scissoring
1433 ()	1437	1440	
1457 (⊥)	1460		
1465 (⊥)	1468	1464	
1470 (⊥)		1480	
2865 ()	2863	2858–2861	CH stretching
2873 (⊥)			
2906 (⊥)	2902	2901–2905	CH_2 symmetric stretching
2925 (⊥)	2923	2921–2926	
2942 (⊥)	2943	2946	
2968 (⊥)	2963	2961	CH_2 asymmetric stretching in tail
2980 ()	2976	2982	CH_2 asymmetric stretching

^a(||) or (⊥) symbols refer to the predicted orientation of the dipole moment vector with respect to the long axis of the 25-OH molecule.

narrower and their intensity upon compression is variable. Narrowing of bands can be assigned to the increase of molecular ordering in Langmuir monolayers in comparison to bulk samples. Since the PM-IRRAS signal intensity increases when the corresponding transition dipole moment is oriented perpendicularly to the surface of water, for Langmuir monolayers, bands from vibrations which are parallel to the long axis of the molecule are usually observed to strengthen (amphiphilic molecules are usually oriented perpendicularly or are slightly inclined to the water surface). In the case of the 25-OH molecule, bands at 2983 cm^{-1} ($\nu_{\text{as}}(\text{CH}_2)$) and 1479 , 1463 , and 1435 cm^{-1} ($\delta_{\text{s}}(\text{CH}_2)$) (for which the dipole moment is oriented parallel to the long axis of the 25-OH molecule) can serve as spectral markers of molecular orientation. The intensity of these bands increases during compression, which suggests that 25-OH molecules are more inclined at lower

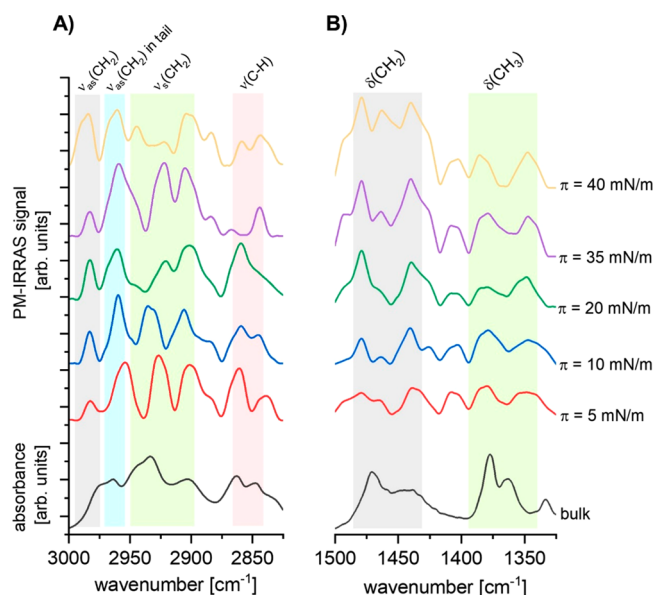


Figure 6. PM-IRRAS spectra for the 25-OH monolayer registered at 20°C compared to the ATR-FTIR spectrum of 25-OH in bulk: hydrocarbon stretching vibrations region (A) and hydrocarbon scissoring vibrations region (B).

values of surface pressure (isotherm region II), and—upon further compression—molecules attain more perpendicular orientation with respect to the water surface. PM-IRRAS spectra recorded at $\pi = 35 \text{ mN/m}$ (isotherm region IV) show a noticeable decrease in intensity of the band at 2983 cm^{-1} , whereas at $\pi = 40 \text{ mN/m}$ (isotherm region V) this peak broadens and its intensity increases. This confirms the earlier conclusion that above the plateau molecules change their orientation and multilayered structures are formed. Additionally, the intensity ratio of bands at 2983 cm^{-1} ($\nu_{\text{as}}(\text{CH}_2)$) observed at different surface pressures (10 and 40 mN/m) is equal to ~ 2.0 , which, again, supports the hypothesis of bilayer formation. More evidence for the existence of this phase transition are changes in mutual intensity and spectral positions of bands attributed to symmetric stretching in CH_2 groups (in the spectral range $2945\text{--}2904 \text{ cm}^{-1}$) as well as in CH groups in the sterane moiety (in the spectral range $2860\text{--}2840 \text{ cm}^{-1}$). At the same time, no significant changes in signals from scissoring vibrations in CH_3 groups (in the spectral range $1383\text{--}1346 \text{ cm}^{-1}$) were observed. This suggests that the observed phase transition is not related to conformational changes in 25-OH molecules.

To get a deeper insight into changes in the chemical environment of hydroxyl groups (at C(3) or C(25)) in the 25-OH molecule observed during compression, spectral bands within the range $1325\text{--}1000 \text{ cm}^{-1}$ (Figure 7) were analyzed.

The PM-IRRAS spectrum recorded at this spectral region shows more diverse absorption bands in comparison to the bulk ATR-FTIR spectrum, which can be explained by the increase of molecular ordering at the water surface. Additionally, some vibration modes may be activated with the changes in the chemical environment around the 25-OH molecule. Unfortunately, bands from C—O—H scissoring vibrations at C(25) and C(3) (observed at 1308 and 1270 cm^{-1} , respectively) are broad and overlap with bands from wagging modes in chains and the sterane moiety. This tendency is particularly noticeable for surface pressure values of $\pi = 35$

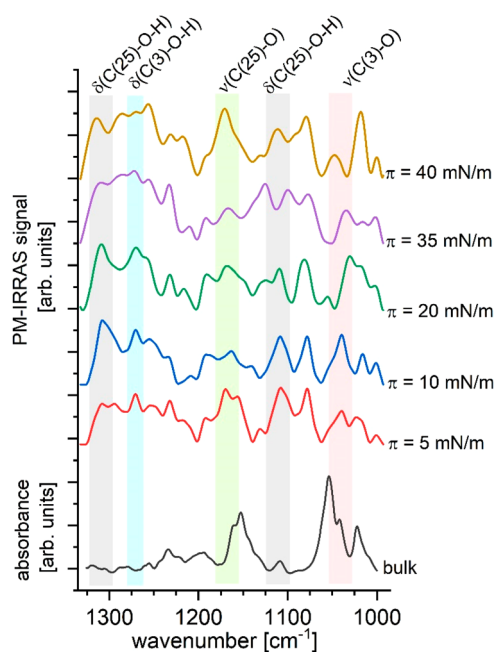


Figure 7. PM-IRRAS spectra for the 25-OH monolayer registered at 20 °C compared to the ATR-FTIR spectrum of 25-OH in bulk in the spectral region 1325–1000 cm^{-1} .

mN/m and $\pi = 40$ mN/m (corresponding to bilayer). This suggests that 25-OH molecules, which were expelled from the monolayer to form the overlayer, adopt different orientations in comparison to those in the layer below (therefore, transition dipole moments of 25-OH molecules from the upper and lower layers are differently oriented and—as a result—narrower bands are observed).

Analysis of bands from C—O stretching vibrations at C(25) and C(3) (observed at 1166 and 1039 cm^{-1} , respectively) brings some valuable observations. Namely, the position of the C(3)—O stretching band maximum shifts during compression (from 5 to 20 mN/m) to lower wavenumbers, which suggests input from additional interactions (probably hydrogen bonding with water molecules). For higher surface pressure values (for $\pi = 35$ and 40 mN/m), this tendency is reversed (the band shifts to higher wavenumbers) and becomes broader, which can suggest that in bilayers the OH group at C(3) can exist in two different environments (interactions with the water surface or neighboring 25-OH molecules). The C(25)—O stretching band is overlapped with various modes (CH_2 wagging and twisting, C=C—C scissoring, and sterane system deformation vibrations); therefore, for lower surface pressure values (for $\pi = 5, 10,$ and 20 mN/m), it is not possible to precisely define peak position. However, it is noticeable that at $\pi = 40$ mN/m the band is shifted to a higher wavenumber. This confirms that in bilayers the hydroxyl group at C(25), similarly to that at C(3), can occur in two different environments (interactions with the water surface or neighboring 25-OH molecules).

3.5. Theoretical Calculations. Considering the experimental study on the 25-OH molecule, two issues remain unclear. The first one is related to the hydrophilicity of hydroxyl groups (one being attached to the sterane system while the other one to the alkyl chain), which may not be equivalent. Former studies revealed that surfactants containing the same polar group attached to the aromatic unit possess

different surface activity as compared to those with a polar group attached to the polymethylene chain.⁵⁸ However, for the 25-OH molecule, the structural effect of the sterane system as well as the resonance between the hydroxyl group (at C(3)) and a double bond in the ring may be insufficient to diversify their surface activity. This is closely related to the second issue concerning the orientation of 25-OH molecules in a monomolecular layer, i.e., by which of the hydroxyl groups (at C(3) or C(25)) the molecule is anchored in the water subphase. Understanding the above issues requires the application of theoretical analysis based on DFT and molecular dynamics calculations. In the first step of our theoretical studies, we intended to obtain information about the preferred anchoring of the 25-OH molecule at the surface of the water. First, the molecular conformation of 25-OH was optimized as well as the energy of hydrogen bonding between a single hydroxyl group (at 25 or 3 positions) and a single water molecule was calculated. The obtained results do not show significant differences in interactions (hydrogen bonding energies calculated for C(3)—OH—water and C(25)—OH—water are comparable, 2.549 and 2.573 kcal/mol, respectively). This suggests that the origin of the 25-OH monolayer formation is mainly associated with the in-plane interactions in the monolayer. Therefore, in the next step, it seemed obvious to examine the thermodynamics of dimer formation with the different mutual orientation of 25-OH molecules. The analyzed dimers were divided into two groups: (i) interacting throughout two hydroxyl groups and (ii) interacting throughout a single hydroxyl group from each molecule (see Figure 8). Among the analyzed mutual arrangements of type

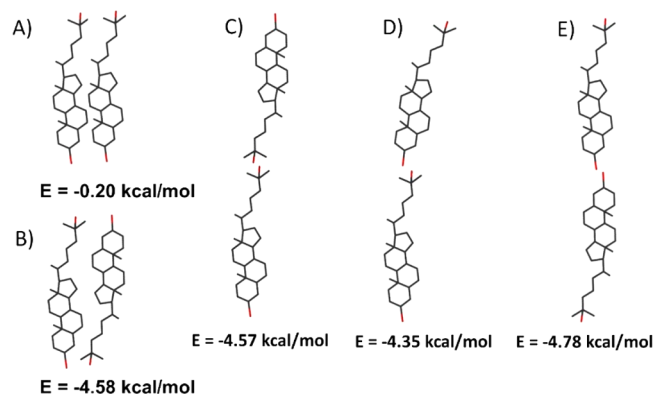


Figure 8. Interaction energy between 25-OH molecules in dimers.

(i) (which corresponds to the monolayer state), the array of staggered molecules is the most favorable. This suggests that oxysterol molecules in the nearest neighbors are anchored to the water surface alternately with one (C(3) or C(25)) hydroxyl group.

In the next step, we performed molecular dynamics simulations to verify this hypothesis. In the theoretical experiment, 25-OH molecules were placed at the surface of the water with different mutual orientations (random (i), anchored with a hydroxyl group at C(3) (ii), or anchored with a hydroxyl group at C(25) (iii)). Then, the production of molecular dynamics was conducted (Figure 9).

The interaction between the oxygen atom from the hydroxyl group connected to the C(3) (or C(25)) atom and water molecules was analyzed using a three-dimensional radial pair distribution function (Figure 9). The radial pair distribution

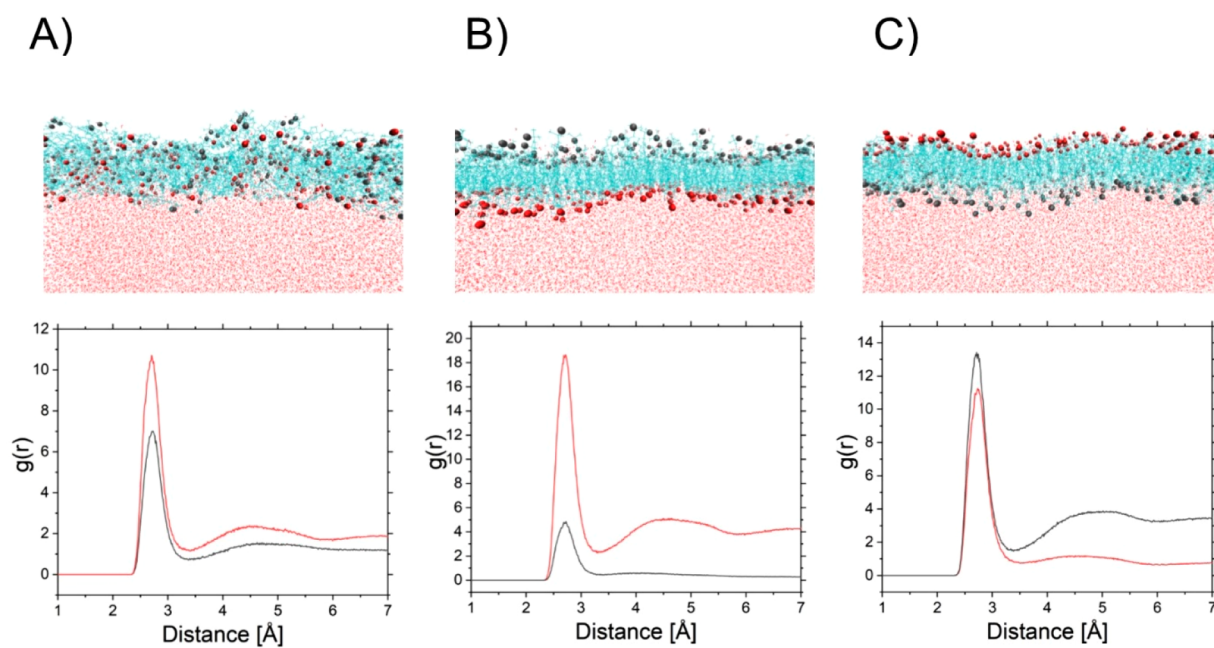


Figure 9. Monolayers obtained after 110 ns production of molecular dynamics for systems with different mutual orientations [random (A), anchored with a hydroxyl group at C(3) (B), or anchored with a hydroxyl group at C(25) (C)]. Red balls and lines represent the hydroxyl group at C(3), and dark gray ones, at C(25). The bottom panel presents the radial pair distribution functions.

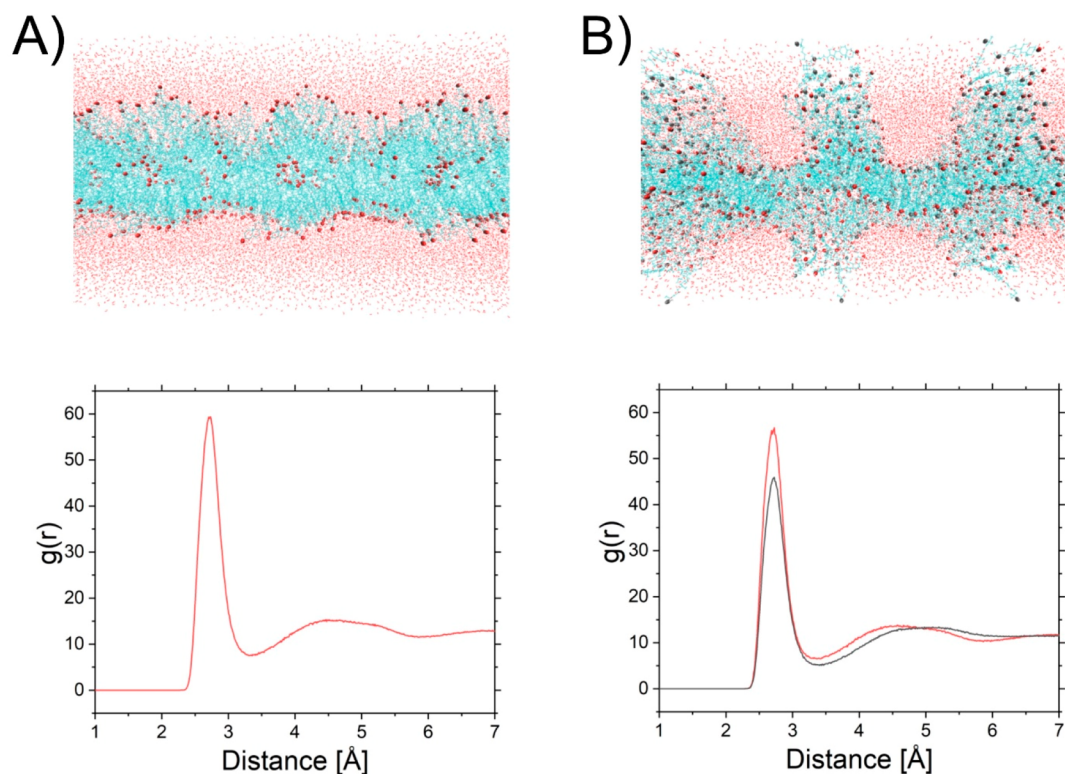


Figure 10. Self-assembling systems of the cholesterol (A) and 25-OH (B) in water after 300 ns production. Red balls and lines represent the hydroxyl group at C(3), and dark gray ones, at C(25). The bottom panel presents the radial pair distribution functions.

function ($g(r)$) calculates the distance (r) between selected atom pairs in each frame of the trajectory. Let us first discuss monolayers with forced, uniform surface anchoring. In the case of molecules anchored with a hydroxyl group at C(3) (ii), the resulting monolayer is smooth and radial pair distribution function values suggest that the hydration of a group at C(3) is higher in comparison to that at C(25). When molecules are

anchored with the hydroxyl group at C(25) (iii), the resulting monolayer becomes folded. Moreover, the analysis of the radial pair distribution plot suggests that hydration of C(25)–OH is higher, however, the difference between hydration of C(25)–OH and C(3)–OH is not as significant as in the case of type (ii). A system with forced anchoring with a hydroxyl group at C(25) drifts to orientation change; therefore, anchoring with

C(3)–OH can be more favorable for the studied system. Analysis of results for a monolayer with randomly oriented molecules (i) verified this hypothesis. The radial pair distribution function plot suggests that, in the obtained film, hydration of C(3)–OH is slightly higher than C(25)–OH. The system (i) did not transform to (ii) despite increased calculation time (to 110 ns). Furthermore, molecular dynamics calculations were conducted for monolayers with defined surface pressure values of 15 and 35 mN/m (see [Supporting Information, Figure S9](#)). As can be noticed, the rise of surface pressure and anchoring in water by C(3) hydroxyl groups induces an increase of molecular ordering in the layer.

Results obtained from molecular dynamics calculations seem to complete the conclusion from simple dimer calculations. The 25-OH molecule at the surface of the water can adopt two different orientations (anchoring alternatively with a hydroxyl group at C(25) or C(3)). However, molecular dynamics simulations suggest that the population of each group is not equal: anchoring with C(3)–OH is more favorable (60% C(3)–OH vs 40% C(25)–OH).

In the next step of our theoretical studies, we analyzed the origin and mechanism of experimentally confirmed bilayer formation. To get a deeper insight into this issue, the results of DFT calculation for dimers of the group (ii) (which corresponds to a bilayer situation) were analyzed. As it can be noticed, there are no significant differences in interaction energy ([Figure 8](#)). More information on the bilayer formation mechanism can be obtained from the simulation of molecular dynamics conducted for a random mixture of cholesterol and water (the first system) and 25-OH and water (the second system) ([Figure 10](#)).

After 300 ns of self-assembly experiment, in the case of cholesterol, a stable bilayer was formed (the obtained bilayer is slightly buckled). For 25-OH, it can be noticed that molecules prefer the formation of a monomolecular layer with more complex protrusions (*branched* monolayers). This can illustrate the process of monolayer–bilayer transition during compression of Langmuir monolayers. It is assumed that protrusions may appear in BAM images as bright filaments and nuclei. In the case of a 25-OH system, radial pair distribution functions for C(25)–OH–O (in water) and C(3)–OH–O (in water) are approximately equal; however, slightly greater hydration of C(3)–OH groups is observed.

4. CONCLUSIONS

In this paper, the behavior of 25-OH at the air/water interface was characterized using a broad spectrum of surface-sensitive techniques. We proved that this compound, in contrast to common bolaamphiphiles, is always anchored with one polar group (either at C(3) or C(25)) to the water surface. The distribution of both orientations is statistical; however, one of them is more favorable. In consequence, a unique phase transition from mono- (2D) to bilayer (3D) was observed and confirmed with optical thickness and PM-IRRAS measurements.

As the phase transition occurs at surface pressure values corresponding to *in vivo* conditions,⁵⁹ our results can be useful to understand differences in biological activity of chain- versus ring-oxidized oxysterols. Although elevated blood levels of oxysterols have mainly been associated with a plethora of pathological conditions (for a review, see [ref 18](#)), recent investigations have also shown their favorable effects related mainly to antiviral properties.⁶⁰ Taking into consideration

representatives of ring-oxidized (7 β -hydroxycholesterol) and chain-oxidized (27- or 25-hydroxycholesterol) sterols, both biological ([ref 60](#) and references therein) and model^{61,62} studies agree that their properties are different. Namely, the latter investigations prove that, depending on the position of the additional hydroxyl group in molecule, both tilt orientation⁶¹ and dynamic properties⁶² are influenced. Biological studies on antiviral potency suggest that ring-substituted hydroxycholesterols (e.g., 7 β -OH) are far less active than 25-OH or 27-OH.⁶⁰ The reason for this phenomenon has not been elucidated so far. We believe that the position of the additional hydroxyl group in the oxysterol molecule may affect miscibility with membrane phospholipids and alter the biomembrane functioning. This aspect of investigations, however, needs further study.

■ ASSOCIATED CONTENT

Supporting Information

The Supporting Information is available free of charge at <https://pubs.acs.org/doi/10.1021/acs.jpcb.9b10938>.

Surface pressure–area isotherms under different experimental conditions; IR spectra of 25-OH; models of monolayers obtained from molecular dynamic calculations ([PDF](#))

■ AUTHOR INFORMATION

Corresponding Author

Patrycja Dynarowicz-Latka – Faculty of Chemistry, Jagiellonian University, 30-387 Kraków, Poland; orcid.org/0000-0002-9778-6091; Email: ucdynaro@cyf-kr.edu.pl

Authors

Anita Wnętrzak – Faculty of Chemistry, Jagiellonian University, 30-387 Kraków, Poland; orcid.org/0000-0002-8086-4647

Anna Chachaj-Brekiesz – Faculty of Chemistry, Jagiellonian University, 30-387 Kraków, Poland; orcid.org/0000-0001-8990-082X

Jan Kobierski – Department of Pharmaceutical Biophysics, Faculty of Pharmacy, Jagiellonian University Medical College, 30-688 Kraków, Poland; orcid.org/0000-0003-3223-0014

Katarzyna Karwowska – Faculty of Chemistry, University of Białystok, 15-425 Białystok, Poland

Aneta D. Petelska – Faculty of Chemistry, University of Białystok, 15-425 Białystok, Poland

Complete contact information is available at: <https://pubs.acs.org/doi/10.1021/acs.jpcb.9b10938>

Notes

The authors declare no competing financial interest.

■ ACKNOWLEDGMENTS

This study was conducted with the use of the KSV PM-IRRAS instrument funded by the European Funds for Regional Development and the National Funds of Ministry of Science and Higher Education, as part of the Operational Program Development of Eastern Poland 2007–2013, project: POPW.01.03.00-20-044/11. This research was supported in part by PL-Grid Infrastructure.

REFERENCES

- (1) Moenke-Wedler, T.; Foerster, G.; Brezesinski, G.; Steitz, R.; Peterson, I. R. Diol Monolayer Structure on the Water Surface and on Solid Substrates. *Langmuir* **1993**, *9*, 2133–2140.
- (2) Aveyard, R.; Binks, B. P.; Cross, A. W.; Fletcher, P. D. I. Dicarboxylic Acids: Stability of Insoluble Monolayers and Ionisation in Langmuir-Blodgett Multilayers. *Colloids Surf., A* **1995**, *98*, 83–91.
- (3) Collins, S. J.; Dhathathreyan, A.; Ramasami, T. Phase Transition in Langmuir Films of Octadecylmalonic Acid. *J. Colloid Interface Sci.* **1998**, *203*, 249–253.
- (4) Nakahara, H.; Nishino, A.; Tanaka, A.; Fujita, Y.; Shibata, O. Interfacial Behavior of Gemini Surfactants with Different Spacer Lengths in Aqueous Medium. *Colloid Polym. Sci.* **2019**, *297*, 183–189.
- (5) Nakahara, H.; Hagimori, M.; Mukai, T.; Shibata, O. Monolayers of a Tetrazine-Containing Gemini Amphiphile: Interplays with Biomembrane Lipids. *Colloids Surf., B* **2018**, *164*, 1–10.
- (6) Hasegawa, T.; Umemura, J.; Takenaka, T. Fourier Transform Infrared Metal Overlayer Attenuated Total Reflection Spectra of Langmuir-Blodgett Films of 12-Hydroxystearic Acid and Its Cadmium Salt. *Thin Solid Films* **1992**, *210–211*, 583–585.
- (7) Vollhardt, D.; Siegel, S.; Cadenhead, D. A. Characteristic Features of Hydroxystearic Acid Monolayers at the Air/Water Interface. *J. Phys. Chem. B* **2004**, *108*, 17448–17456.
- (8) Siegel, S.; Vollhardt, D.; Cadenhead, D. A. Effect of the Hydroxyl Group Position on the Monolayer Characteristics of Hydroxypalmitic Acids. *Colloids Surf., A* **2005**, *256*, 9–15.
- (9) Vollhardt, D.; Siegel, S.; Cadenhead, D. A. Effect of Hydroxyl Group Position and System Parameters on the Features of Hydroxystearic Acid Monolayers. *Langmuir* **2004**, *20*, 7670–7677.
- (10) Vollhardt, D.; Fainerman, V. B. Effect of the Hydroxyl Group Position on the Phase Behavior of Hydroxyoctadecanoic Acid Monolayers at the Air/Water Interface. *J. Phys. Chem. B* **2004**, *108*, 297–302.
- (11) Kellner, B. M. J.; Cadenhead, D. A. Monolayer Studies of Hydroxyhexadecanoic Acids. *J. Colloid Interface Sci.* **1978**, *63*, 452–460.
- (12) Menger, F. M.; Richardson, S. D.; Wood, M. G.; Sherrod, M. J. Chain-Substituted Lipids in Monomolecular Films. Effect of Polar Substituents on Molecular Packing. *Langmuir* **1989**, *5*, 833–838.
- (13) Huda, M. S.; Fujio, K.; Uzu, Y. Phase Behavior of Bipolar Fatty Acid Monolayers. *Bull. Chem. Soc. Jpn.* **1996**, *69*, 3387–3394.
- (14) Vogel, V.; Möbius, D. Reorganization of Bipolar Lipid Molecules in Monolayers at the Air/Water Interface. *Thin Solid Films* **1985**, *132*, 205–219.
- (15) Legre, J. P.; Albinet, G.; Caille, A. Models for the Phase Transition in a Monolayer of Amphiphilic Bipolar Molecules on an Aqueous Substrate. *Can. J. Phys.* **1982**, *60*, 893–900.
- (16) Fuhrhop, J. H.; David, H. H.; Mathieu, J.; Liman, U.; Winter, H. J.; Boekema, E. Bolaamphiphiles and Monolayer Lipid Membranes Made from 1,6,19,24-Tetraoxa-3,21-Cyclohexatriacontadiene-2,5,20,23-Tetrone. *J. Am. Chem. Soc.* **1986**, *108*, 1785–1791.
- (17) Bakowsky, U.; Rothe, U.; Antonopoulos, E.; Martini, T.; Henkel, L.; Freisleben, H. J. Monomolecular Organization of the Main Tetraether Lipid from Thermoplasma Acidophilum at the Water-Air Interface. *Chem. Phys. Lipids* **2000**, *105*, 31–42.
- (18) Kulig, W.; Cwiklik, L.; Jurkiewicz, P.; Rog, T.; Vattulainen, I. Cholesterol Oxidation Products and Their Biological Importance. *Chem. Phys. Lipids* **2016**, *199*, 144–160.
- (19) Brown, A. J.; Jessup, W. Oxysterols: Sources, Cellular Storage and Metabolism, and New Insights into Their Roles in Cholesterol Homeostasis. *Mol. Aspects Med.* **2009**, *30*, 111–122.
- (20) Gill, S.; Chow, R.; Brown, A. J. Sterol Regulators of Cholesterol Homeostasis and beyond: The Oxysterol Hypothesis Revisited and Revised. *Prog. Lipid Res.* **2008**, *47*, 391–404.
- (21) Olkkonen, V. M.; Hynynen, R. Interactions of Oxysterols with Membranes and Proteins. *Mol. Aspects Med.* **2009**, *30*, 123–133.
- (22) Pusterla, J. M.; Malfatti-Gasperini, A. A.; Puentes-Martinez, X. E.; Cavalcanti, L. P.; Oliveira, R. G. Refractive Index and Thickness Determination in Langmuir Monolayers of Myelin Lipids. *Biochim. Biophys. Acta, Biomembr.* **2017**, *1859*, 924–930.
- (23) Winsel, K.; Hönig, D.; Lunkenheimer, K.; Geggel, K.; Witt, C. Quantitative Brewster Angle Microscopy of the Surface Film of Human Broncho-Alveolar Lavage Fluid. *Eur. Biophys. J.* **2003**, *32*, 544–552.
- (24) Frisch, M. J.; Trucks, G. W.; Schlegel, H. B.; Scuseria, G. E.; Robb, M. A.; Cheeseman, J. R.; Scalmani, G.; Barone, V.; Petersson, G. A.; Nakatsuji, H.; et al. *Gaussian 16*, revision B.01; Gaussian, Inc.: Wallingford, CT, 2016.
- (25) Becke, A. D. Density-functional Thermochemistry. III. The Role of Exact Exchange. *J. Chem. Phys.* **1993**, *98*, 5648–5652.
- (26) Lee, C.; Yang, W.; Parr, R. G. Development of the Colle-Salvetti Correlation-Energy Formula into a Functional of the Electron Density. *Phys. Rev. B: Condens. Matter Mater. Phys.* **1988**, *37*, 785–789.
- (27) Vosko, S. H.; Wilk, L.; Nusair, M. Accurate Spin-Dependent Electron Liquid Correlation Energies for Local Spin Density Calculations: A Critical Analysis. *Can. J. Phys.* **1980**, *58*, 1200–1211.
- (28) Stephens, P. J.; Devlin, F. J.; Chabalowski, C. F.; Frisch, M. J. Ab Initio Calculation of Vibrational Absorption and Circular Dichroism Spectra Using Density Functional Force Fields. *J. Phys. Chem.* **1994**, *98*, 11623–11627.
- (29) Precomputed vibrational scaling factors; <https://cccbdb.nist.gov/vibscalejust.asp>.
- (30) Wang, J.; Wang, W.; Kollman, P. A.; Case, D. A. Automatic Atom Type and Bond Type Perception in Molecular Mechanical Calculations. *J. Mol. Graphics Modell.* **2006**, *25*, 247–260.
- (31) Wang, J.; Wolf, R. M.; Caldwell, J. W.; Kollman, P. A.; Case, D. A. Development and Testing of a General Amber Force Field. *J. Comput. Chem.* **2004**, *25*, 1157–1174.
- (32) Martínez, L.; Andrade, R.; Birgin, E. G.; Martínez, J. M. PACKMOL: A Package for Building Initial Configurations for Molecular Dynamics Simulations. *J. Comput. Chem.* **2009**, *30* (13), 2157–2164.
- (33) Jorgensen, W. L.; Chandrasekhar, J.; Madura, J. D.; Impey, R. W.; Klein, M. L. Comparison of Simple Potential Functions for Simulating Liquid Water. *J. Chem. Phys.* **1983**, *79*, 926–935.
- (34) Case, D. A.; Cerutti, D. S.; Cheatham, T. E. L.; Darden, T. A.; Duke, R. E.; Giese, T. J.; Gohlke, H.; Goetz, A. W.; Greene, D.; Homeyer, N.; et al. *Amber 2018*; University of California, San Francisco: 2018.
- (35) Dickson, C. J.; Madej, B. D.; Skjevik, Å. A.; Betz, R. M.; Teigen, K.; Gould, I. R.; Walker, R. C. Lipid14: The Amber Lipid Force Field. *J. Chem. Theory Comput.* **2014**, *10*, 865–879.
- (36) Humphrey, W.; Dalke, A.; Schulten, K. VMD: Visual Molecular Dynamics. *J. Mol. Graphics* **1996**, *14*, 33–38.
- (37) Roe, D. R.; Cheatham, T. E. PTRAJ and CPPTRAJ: Software for Processing and Analysis of Molecular Dynamics Trajectory Data. *J. Chem. Theory Comput.* **2013**, *9*, 3084–3095.
- (38) Janout, V.; Turkyilmaz, S.; Wang, M.; Wang, Y.; Manaka, Y.; Regen, S. L. An Upside down View of Cholesterol's Condensing Effect: Does Surface Occupancy Play a Role? *Langmuir* **2010**, *26*, 5316–5318.
- (39) Theunissen, J. J. H.; Jackson, R. L.; Kempen, H. J. M.; Demel, R. A. Membrane Properties of Oxysterols. Interfacial Orientation, Influence on Membrane Permeability and Redistribution between Membranes. *Biochim. Biophys. Acta, Biomembr.* **1986**, *860*, 66–74.
- (40) Kauffman, J. M.; Westerman, P. W.; Carey, M. C. Fluorocholesterols, in Contrast to Hydroxycholesterols, Exhibit Interfacial Properties Similar to Cholesterol. *J. Lipid Res.* **2000**, *41*, 991–1003.
- (41) Mintzer, E.; Charles, G.; Gordon, S. Interaction of Two Oxysterols, 7-Ketocholesterol and 25-Hydroxycholesterol, with Phosphatidylcholine and Sphingomyelin in Model Membranes. *Chem. Phys. Lipids* **2010**, *163*, 586–593.
- (42) Vollhardt, D.; Fainerman, V. B. New Aspects in the Consideration of Compressibility for the Characterization of

Langmuir Monolayers. *Interfacial Rheology*; CRC Press: 2009; pp 429–475.

(43) Fukuto, M.; Heilmann, R. K.; Pershan, P. S.; Yu, S. M.; Griffiths, J. A.; Tirrell, D. A. Structure of Poly(γ -Benzyl-L-Glutamate) Monolayers at the Gas-Water Interface: A Brewster Angle Microscopy and x-Ray Scattering Study. *J. Chem. Phys.* **1999**, *111*, 9761–9777.

(44) Baglioni, P.; Cestelli, O.; Dei, L.; Gabrielli, G. Monolayers of Cholesterol at Water-Air Interface: Mechanism of Collapse. *J. Colloid Interface Sci.* **1985**, *104*, 143–150.

(45) Fidalgo Rodriguez, J. L.; Caseli, L.; Minones Conde, J.; Dynarowicz-Latka, P. New Look for an Old Molecule – Solid/Solid Phase Transition in Cholesterol Monolayers. *Chem. Phys. Lipids* **2019**, *225*, 104819.

(46) Benedini, L.; Fanani, M. L.; Maggio, B.; Wilke, N.; Messina, P.; Palma, S.; Schulz, P. Surface Phase Behavior and Domain Topography of Ascorbyl Palmitate Monolayers. *Langmuir* **2011**, *27*, 10914–10919.

(47) Fanani, M. L.; Maggio, B. Phase State and Surface Topography of Palmitoyl-Ceramide Monolayers. *Chem. Phys. Lipids* **2010**, *163*, 594–600.

(48) Toimil, P.; Prieto, G.; Miñones, J.; Sarmiento, F. A Comparative Study of F-DPPC/DPPC Mixed Monolayers. Influence of Subphase Temperature on F-DPPC and DPPC Monolayers. *Phys. Chem. Chem. Phys.* **2010**, *12*, 13323–13332.

(49) Rapaport, H.; Kuzmenko, I.; Lafont, S.; Kjaer, K.; Howes, P. B.; Als-Nielsen, J.; Lahav, M.; Leiserowitz, L. Cholesterol Monohydrate Nucleation in Ultrathin Films on Water. *Biophys. J.* **2001**, *81*, 2729–2736.

(50) Phan, M. D.; Lee, J.; Shin, K. Collapsed States of Langmuir Monolayers. *J. Oleo Sci.* **2016**, *65*, 385–397.

(51) Lee, K. Y. C. Collapse Mechanisms of Langmuir Monolayers. *Annu. Rev. Phys. Chem.* **2008**, *59*, 771–791.

(52) Dynarowicz-Latka, P.; Dhanabalan, A.; Oliveira, O. N. Modern Physicochemical Research on Langmuir Monolayers. *Adv. Colloid Interface Sci.* **2001**, *91*, 221–293.

(53) Morgan, H.; Martin Taylor, D.; Oliveira, O. N. Proton Transport at the Monolayer-Water Interface. *Biochim. Biophys. Acta, Biomembr.* **1991**, *1062*, 149–156.

(54) Oliveira, O. N.; Bonardi, C. The Surface Potential of Langmuir Monolayers Revisited. *Langmuir* **1997**, *13*, 5920–5924.

(55) Sacconi, J.; Castano, S.; Beaurain, F.; Laguerre, M.; Desbat, B. Stabilization of Phospholipid Multilayers at the Air–Water Interface by Compression beyond the Collapse: A BAM, PM-IRRAS, and Molecular Dynamics Study. *Langmuir* **2004**, *20*, 9190–9197.

(56) Röefzaad, M.; Klüner, T.; Brand, I. Orientation of the GM1 Ganglioside in Langmuir-Blodgett Monolayers: A PM IRRAS and Computational Study. *Phys. Chem. Chem. Phys.* **2009**, *11*, 10140–10151.

(57) Goto, T. E.; Caseli, L. Understanding the Collapse Mechanism in Langmuir Monolayers through Polarization Modulation-Infrared Reflection Absorption Spectroscopy. *Langmuir* **2013**, *29*, 9063–9071.

(58) van Os, N. M.; Kok, R.; Bolsman, T. A. B. M. Alkylarenesulphonates: The Effect of Chemical Structure on Physico-Chemical Properties. *Tenside, Surfactants, Deterg.* **1992**, *29*, 175–189.

(59) Marsh, D. Lateral Pressure Profile, Spontaneous Curvature Frustration, and the Incorporation and Conformation of Proteins in Membranes. *Biophys. J.* **2007**, *93*, 3884–3899.

(60) Lembo, D.; Cagno, V.; Civra, A.; Poli, G. Oxysterols: An Emerging Class of Broad Spectrum Antiviral Effectors. *Mol. Aspects Med.* **2016**, *49*, 23–30.

(61) Kulig, W.; Olżyńska, A.; Jurkiewicz, P.; Kantola, A. M.; Komulainen, S.; Manna, M.; Pourmousa, M.; Vazdar, M.; Cwiklik, L.; Rog, T.; et al. Cholesterol under Oxidative Stress - How Lipid Membranes Sense Oxidation as Cholesterol is Being Replaced by Oxysterols. *Free Radical Biol. Med.* **2015**, *84*, 30–41.

(62) Kulig, W.; Mikkolainen, H.; Olżyńska, A.; Jurkiewicz, P.; Cwiklik, L.; Hof, M.; Vattulainen, I.; Jungwirth, P.; Rog, T. Bobbing of Oxysterols: Molecular Mechanism for Translocation of Tail-Oxidized

Sterols through Biological Membranes. *J. Phys. Chem. Lett.* **2018**, *9*, 1118–1123.